This is an *Accepted Manuscript*, which has been through the Royal Society of Chemistry peer review process and has been accepted for publication.

Accepted Manuscripts are published online shortly after acceptance, before technical editing, formatting and proof reading. Using this free service, authors can make their results available to the community, in citable form, before we publish the edited article. We will replace this *Accepted Manuscript* with the edited and formatted *Advance Article* as soon as it is available.

You can find more information about *Accepted Manuscripts* in the **Information for Authors**.

Please note that technical editing may introduce minor changes to the text and/or graphics, which may alter content. The journal's standard **Terms & Conditions** and the **Ethical guidelines** still apply. In no event shall the Royal Society of Chemistry be held responsible for any errors or omissions in this *Accepted Manuscript* or any consequences arising from the use of any information it contains.

ChemComm

Dynamic Article Links ▶

COMMUNICATION

Synthesis of Concave Gold Nanocuboids with High-index Facets and Their Enhanced Catalytic Activity†

Lidong Li, Yi Peng, Yonghai Yue,* Ye Hu, Xiu Liang, Penggang Yin, and Lin Guo*

Abstract: Novel concave gold nanocuboids bounded by 24 high-index {611} facets are synthesized using seed-mediated growth method via an overgrowth mechanism. The as-synthesized products demonstrated greatly enhanced
10 **catalytic activity for the electro-oxidation of glucose and the reduction of 4-nitrothiophenol (4-NTP) under a laser.**

The development of novel nanomaterials progresses the fundamental research and practical applications in catalytics[1]. In the past decade, numerous novel face-centered cubic (fcc)
15 metallic materials have been synthesized into a variety of nanostructures, such as cubes, octahedrons, decahedrons, rods, etc.[2] Theoretically, all of these structures are enclosed by low-index facets, such as {111}, {100} or {110} crystallographic facets. Nanocrystals enclosed by high-index facets with a large
20 density of atomic steps, kinks and dangling bonds are highly expected. So far, several new types of nanocrystals enclosed by high-index facets have recently been developed. For example, Sun et al. first reported the preparation of tetrahexahedral (THH) platinum nanocrystals enclosed by 24 high-index facets, such as
25 {730} or {520}, using an electrochemical method.[3] Murphy et al. and El-Sayed et al.[2a, 2b, 4] synthesized THH gold nanocrystals with {520} high-index facets using a modified seed-mediated growth process. Mirkin et al. continued improving the seed-mediated growth process by replacing the surfactants and obtained concave
30 cubic Au NCs enclosed by 24 high-index {720} facets.[5] Compared with high-index faceted nanocrystals with convex surfaces, concave structures are attractive for a wide variety of applications in electrochemical catalysis, plasmonics, surface-enhanced Raman spectroscopy (SERS), etc. This interest arises
35 from their high-index facets, surface cavities and sharp corners/edges. However, because generating and stabilizing a concave surface with negative curvature is not thermodynamically favorable; significantly more energy is required to produce a concave structure than its convex
40 counterpart, the synthesis of nanocrystals with a concave structure is still challenging and remains in an early stage of development.

Herein, we report a new approach to synthesize concave gold nanocuboids (concave Au NCs) enclosed by 24 {611} high-index
45 facets using an improved seed-mediated growth method. We carefully investigated the effect of didodecyldimethylammonium bromide (DDAB) and ascorbic acid (AA) concentration on the morphology of the final products. Typically, increasing the

DDAB concentration facilitates the formation of concave
50 structures through an overgrowth mechanism, whereas increasing the amount of AA results in a more kinetic-controlled process. Because of their high-index facets, the concave Au NCs demonstrated significantly enhanced catalytic activity for the electro-oxidation of glucose and increased in situ catalytic
55 activity for the reduction of 4-NTP using SERS. Compared with previously published work related to concave Au nanocrystals with high-index facets[5,6], our approach is simpler, and both electrocatalytic and SERS activities are investigated in detail.

The as-synthesized products were extensively characterized by
60 SEM and TEM (as shown in figure 1). A closer examination indicates that almost all the cubes were somewhat elongated along one of the axes to form rectangular bars with aspect ratios slightly larger than one, therefore, we called the products nanocuboids instead of nanocubes. Additionally, the SEM image
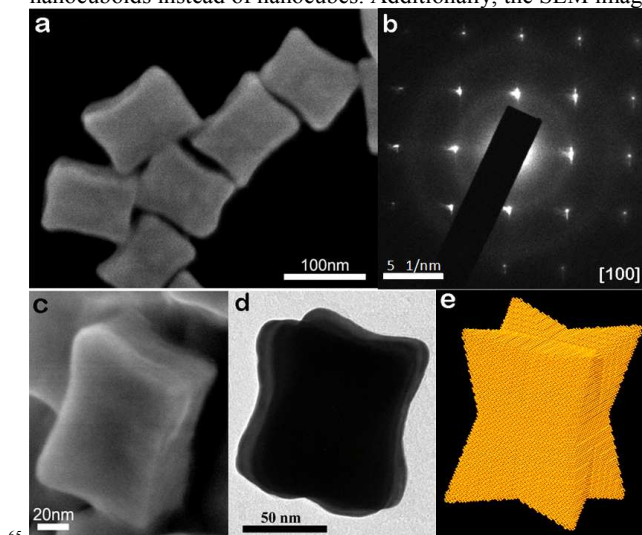

65 Figure 1. (a) A SEM image showing the morphology and size of concave Au NCs. (b) The SAED pattern of a single particle measured from the [100] zone axis (c-d) High-magnification SEM and TEM images of a single concave gold nanocuboid (e) A
70 3D model of a concave Au NC.

(figure S1) of a dispersed single layer of concave Au NCs displays a high purity product yield. The selected-area electron diffraction (SAED) pattern shown in figure 1b reveals the single crystal nature of the products, and the calculated lattice constant

is 4.078Å. As shown in figure 1c-d, each nanocuboid exhibits darker contrast in the middle region as compared with a edge, further verifying its concave structure. The average size of concave Au NC was measured to be approximately 100±10 nanometers. The three-dimensional (3D) model for the concave Au NC structure is presented in figure 1e.

To further study the exposed high-index facets of the products, HRTEM images was taken from [110] direction. Herein, for this specific concave structure, the concave facets or side edges can be directly captured as shown in figure 2a. As shown in Figure 2c-d, a typical series of {551} high-index planes along the [110] zone axis was captured in the HRTEM images of the boxed region in figure 2b. Of note, the {551} high-index plane was on
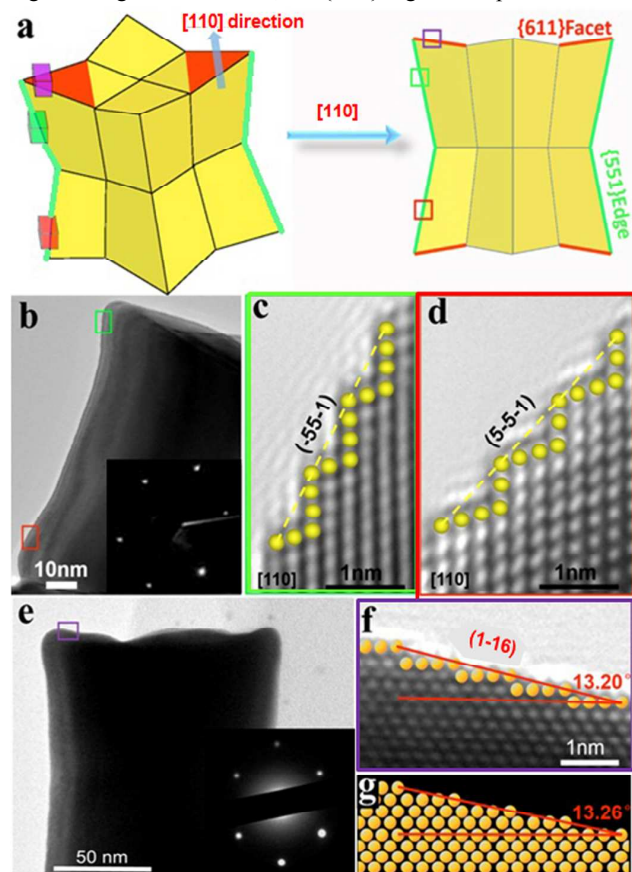
the edge of the concave Au NC and not on the concave surface (as shown in figure 2a). To exactly index the concave facet for each concave surface, the other side of the nanocrystal that directly projects the facet according to the 3D model shown in figure 2a along the [110] zone axis was also measured. Figure 2f displays the HRTEM image of the boxed region in figure 2e, and

a series of high-index {611} plane are clearly observed. The angle measurement of 13.20° measured between [200] and the marked side is similar to the calculated theoretical value (13.26°) (Figure 2g) and indicates a high-index {611} facet. From Figure S2, the measured angle of 11.49° recorded from the [001] zone axis is very close to the measured angle of 11.58° recorded from [100] zone axis, which indicates that the included angles of any two of the three edges for each cuboid corner are the same, resulting in an overall profile indexed as the {551} side edges and the {611} concave facets. And this observed result is perfectly consistent with the calculated result that two intersecting {551} side edges can form a {611} facet in space, which further verify the above structure analysis of the concave Au NCs.

In addition, to index a concave facet, taking a cross section view of a concave crystal is always helpful. Herein, we utilized ultrathin section method to prepare samples with their normal directions along the cuboids' <110> direction. The remaining section was then tilted to the [110] direction to show the top view of the concave structure (as shown in figure 3a). The projected images of (Figure 3c) fit well with the model (Figure 3a) except for slightly bumped regions, which are probably due to the big thickness of the cross section (thickness: 30 nm) compared to the size of the samples (~90 nm). Figure 3d displays the HRTEM image of the boxed region in figure 3b, and a series of high-index {611} planes are clearly observed. The measured angle is 13.29°, indicating that the facets of the concave cuboids are indeed high-index {611} facets, which have a calculated angle of 13.26°. The structure of the proposed concave gold nanocuboids is further confirmed by consistent SAED patterns and the HRTEM images of individual concave Au NCs from different zone axes,
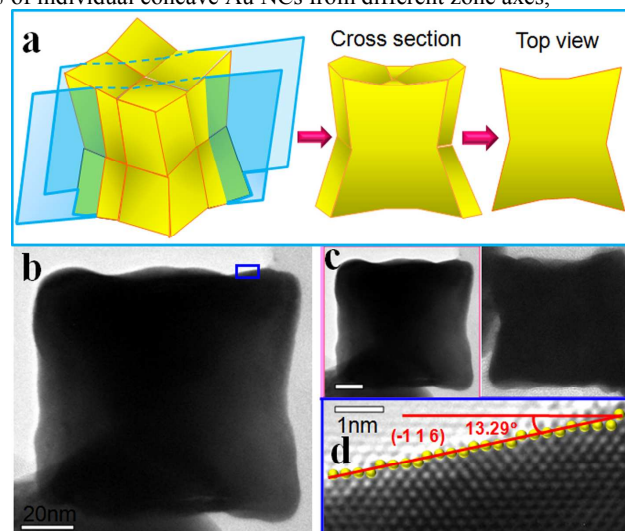

Figure 3. (a) Model of cross-sectioned concave nanocuboids. (b) Zoomed-in image of a single cut concave cuboid aligned edge-on. (c) TEM images of cross-sectioned concave cuboids (scale bar: 20 nm). (d) HRTEM image of the boxed region in figure 4c exhibiting a series of high-index {611} concave facets.

including the [001], [100], [110] and [011] zone axes (Figure S3). On the basis of above structural analysis, we conclude that the concave Au NCs are mainly enclosed by 24 high-index {611} facets and 24 {551} side edges except for the rounded corners.

To further understand the growth mechanism of the concave

Au NCs, the following two control experiments were conducted: 1) the amount of DDAB surfactant was varied and 2) the quantity of AA reducing agent was adjusted. For DDAB concentrations of 5 mM, 10 mM and 15 mM, rhombic dodecahedrons (RDs)
5 enclosed by {110} facets,[2c] concave cuboids enclosed by {611} facets, and trioctahedron (TOHs) enclosed by {221} facets were obtained,[7] respectively, as shown in figure 4a-c. Increasing the concentration of DDAB facilitated the formation of concave structures. Small concave indentations were observed and are
10 denoted on the RDs in figure 4a, whereas appreciable concave structures were observed for the concave Au NCs and, to an even greater extent, for the TOHs (figure 4c). To verify the morphological transition during synthesis, TEM images of the
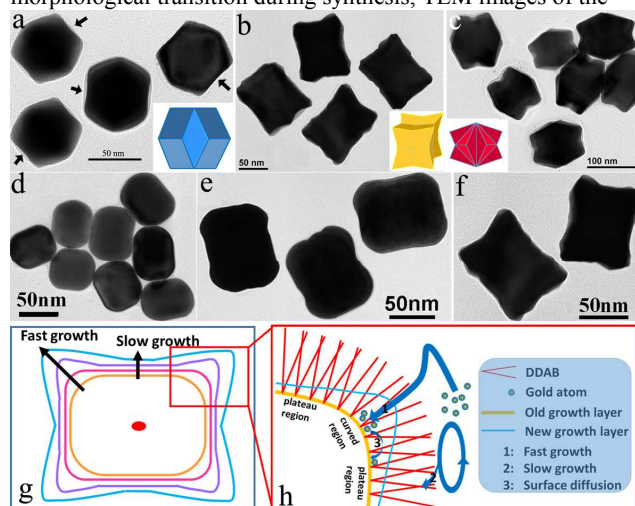

15 Figure 4. (a-c) The products formed using varying concentrations of DDAB. (a) RDs enclosed by {110} facets with a 5 mM DDAB concentration. (b) Concave cuboids enclosed by {611} high-index facets with a 10 mM DDAB concentration. (c) TOHs enclosed by {221} facets with a 15 mM DDAB concentration. (d-
20 f) TEM images of products at various times during the growth process: (d) capsule nanocrystals at 3 h, (e) quasi-concave nanocuboids at 4.5 h, and (f) concave Au NCs at 6 h. (g-h) Schematic of overgrowth mechanism at curved regions (the <111> orientation) that describes the synthesis of concave Au
25 NCs with controlled quantities of DDAB and AA.

products at various stages were obtained. As the reaction time increased from 3 to 4.5 h, the capsule nanocrystals gradually evolved into quasi-concave nanocuboids and then concave Au NCs after 6 h growth (figure 4d-f). Additionally, the gradual red
30 shift from 530 nm to 620 nm in the UV-Vis spectrum sampled at different stages confirms the formation of concave structures (figure S4). Furthermore, figure 4g-h illustrates the overgrowth mechanism of concave Au NCs. Two-dimensional growth layers are illustrated in figure 4g according to the morphologies
35 observed at various stages. This confirms that the formation of concave structures is attributed to the overgrowth mechanism because growth along the <111> orientation occurred faster than growth along the <100> orientation. From the schematic presented in figure 4h, we hypothesize that DDAB is essential
40 because it possesses a double C12 hydrophobic tail. Steric hindrance occurs when two large organic tails are absorbed on a crystal surface. Steric hindrance is more pronounced at plateau

regions than at regions with higher curvature. Therefore, newly formed gold atoms are expected to nucleate and grow on curved
45 surfaces rather than flat surfaces. Although atoms diffused on the surface from curved regions to flat regions, growth along the <111> orientation tended to be faster than growth along the <100> or <110> orientations, which resulted in concave gold nanocuboids enclosed by {611} high-index facets. Meanwhile,
50 when a small amount of AA (80 μL) was added to the growth solution, the reduction rate was relatively low and the newly formed Au atoms had sufficient time to migrate to other sites, such as the edges or side faces, after being deposited. Therefore, the relatively convex morphology of typical icosahedrons was
55 obtained (figure S5a). Because a faster reduction rate is expected with increasing amounts of AA (160 μL), the probability of atoms migrating from corner sites to side faces is quite low. Growth is expected to predominately occur along the <111> direction to obtain concave cuboid structures (figure 1a). At even higher
60 reduction rates, when the AA amount was increased to 200μL, significant overgrowth on the corners was observed and a flower-like morphology was produced (figure S5b). The DDAB provided an appropriate soft concave structure template and the AA imparted a suitable reduction rate, which resulted in the
65 formation of concave Au NCs with {611} high-index facets via an overgrowth mechanism.

Because there are a high density of atomic steps and kinks on {611} facets, concave Au NCs are expected to exhibit increased chemical activity, which was demonstrated by the oxidation
70 peaks from the cyclic voltammetry (CV) curves for concave gold nanocuboids and spherical gold nanoparticles (Au NPs, figure S6) in H_2SO_4 at 1.15-1.51 V and 1.27-1.57 V, respectively (figure S7). The oxidation peak, which was at a lower potential for concave Au NCs than spherical Au NPs, indicates that the surface atoms
75 of the concave Au NCs are more easily oxidized. The current densities were normalized to the electrochemically active surface area (EASA), and the results indicate that the EASA of concave Au NCs is 3.19 times larger than that of spherical AuNPs (figure S7). The electro-catalytic properties were measured in a glucose
80 solution. Figure 5a compares the CV curves for the electro-oxidation of glucose using modified Au NP and concave Au NC catalysts on a glassy carbon electrode (GCE). The peak current density of glucose oxidation at 0.24 V (vs. Ag/AgCl) during a positive potential scan was 0.51 mA·cm^{-2} and 6.01 mA·cm^{-2} for
85 Au NPs and concave Au NCs, respectively, which indicates that the catalytic activity of concave Au NCs is 11.8 times greater than that of spherical Au NPs. Figure 5b presents the chronoamperometry (CA) curves for the electro-oxidation of glucose at 0.24 V over 180 s. At the plateau region, the current
90 density of the Au NPs and concave Au NCs was 0.24 mA·cm^{-2} and 2.434 mA·cm^{-2}, respectively, which suggests that the activity of concave Au NCs is 10 times greater than the catalytic activity of Au NPs. The stability of the electro-catalytic activity of concave Au NCs is demonstrated by the CV curves, which
95 maintained more than 95% of their initial value after 100 potential cycles (figure S8). These results reveal that concave Au NCs are efficient catalysts that may be utilized to produce electrical energy from glucose biofuel cells, which is a green method because glucose is a reproducible biofuel found in most
100 plants.

In addition, the greatly enhanced catalytic properties of concave Au NCs can also be demonstrated by SERS, because this structure can provide much stronger plasmon signals. In this approach, a self-assembled monolayer of 4-NTP can be
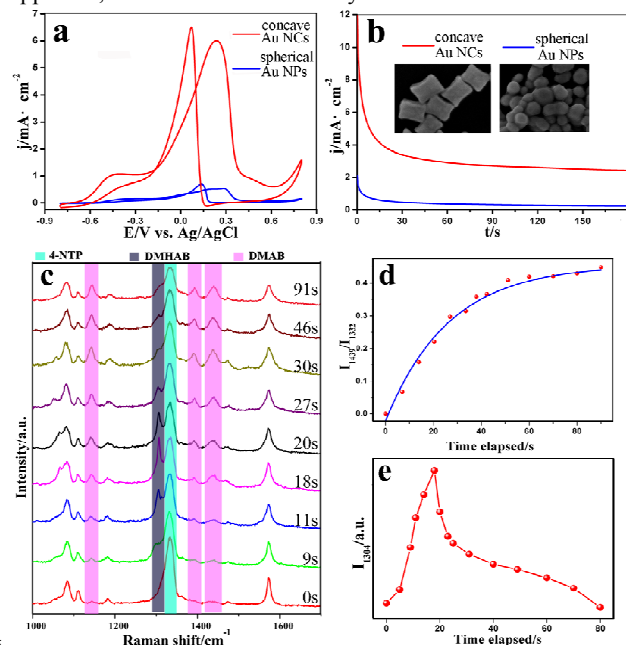

Figure 5. (a) CV curves of spherical Au NPs and concave Au NCs modified on GCE in a 0.1 M NaOH solution of 10 mM glucose at a scan rate of 50 mV•s^{-1}. (b) I-t curves for glucose oxidation measured on spherical Au NPs and concave Au NCs at 0.24 V over 180 s. (c) SERS spectra of 4-NTP absorbed on concave Au NCs recorded over various periods of time. (d) The time relative SERS intensity ratio of the 1439 cm^{-1} to 1143 cm^{-1} bands indicates the catalytic reduction reaction. (e) The time relative SERS intensity at 1304 cm^{-1} indicates the change in the intermediate product of the reduction reaction.

catalytically reduced in situ on the surface of concave Au NCs to produce dimercaptoazobenzene (DMAB) under a 632.8 nm laser. The process of catalytic reduction can be directly characterized by time-dependent SERS spectra recorded over different periods of time. Figure 5c shows a typical SERS spectrum of the system during the reaction under a 0.3 mW laser. The gradually increasing vibrational Raman bands at 1143, 1393, and 1439 cm^{-1} (highlighted by three pink bands in figure 5c) attributed to C-N symmetric stretching, N=N stretching, and C-H in-plane bending modes, respectively, can be assigned to the production of DMAB, whereas the gradually decreasing vibrational Raman band at 1332 cm^{-1} (highlighted by the blue band in figure 5c), representing NO$_2$ symmetric stretching, and the unchanged peaks at 1080 and 1573 cm^{-1}, attributed to phenyl ring modes, can be assigned to either 4-NTP or DMAB[8]. As shown in figure 5d, the relative intensities of 1439 and 1332 cm^{-1} were selected as quantitative measures of the conversion of 4-NTP, and the time dependent relative intensities of the bands clearly indicate that the quantity of DMAB initially increases rapidly before reaching a maximum value and leveling off at I$_{1439}$/I$_{1332}$=0.42. Furthermore, we measured a Raman band at 1306 cm^{-1} (highlighted by the gray band in figure 5c) for the first time that possibly can be assigned

to the formation of intermediate dimercaptohydrazobenzene (DMHAB) products. As shown in the spectra collected at varying times and the intensity changes observed at 1306 cm^{-1} (figure 5e), the band appeared after 9 s of laser irradiation before it rapidly increased. After reaching the highest intensity at 18 s, the Raman band diminished quickly. This indicates the mechanism that produces DMAB from 4-NTP through intermediate DMHAB products. However, when concave Au NCs were replaced with spherical Au NPs, only slight changes were observed over longer periods of time under the same laser power (figure S9), which indicates that the large density of steps and kinks in the exposed {611} high-index facets and the sharp corners of the concave Au nanocuboids are responsible for the significantly enhanced catalytic reduction of 4-NTP. At a higher laser power, such as 4 mW, more DMAB was produced (I$_{1439}$/I$_{1332}$=0.83). Additionally, the intermediate DMHAB products were difficult to be observed because the reaction occurred too quickly (figure S10).

Conclusions

In summary, novel concave gold nanocuboids with 24 exposed {611} high-index facets were successfully synthesized using an improved seed-mediated growth method. Both DDAB and AA were demonstrated to be critical factors in the <111> overgrowth mechanism. The catalytic activity per unit surface area of concave Au NCs for the electro-oxidation of glucose was determined to be more than 10 times higher than that of spherical gold nanoparticles. Additionally, the concave Au NCs demonstrated significantly enhanced catalytic activity for the reduction of 4-NTP, which was monitored in situ using time-dependent SERS. Taken all together, this novel concave nanocuboid structure with {611} high-index facets may be a potential candidate for future catalytic studies.

Notes and references

* School of Chemistry and Environment, Beihang University, Beijing, 100191, P. R. China. E-mail:yueyonghai@buaa.edu.cn (Yue, Y), guolin@buaa.edu.cn (Guo, L)

1   a) H. Zhang, M. Jin, Y. Xia, *Chem. Soc. Rev.* 2012, **41**, 8035; b) H. You, S. Yang, B. Ding, H. Yang, *Chem. Soc. Rev.* 2013, **42**, 2880.

2   a) N. R. Jana, L. Gearheart, C. J. Murphy, *J. Phys. Chem. B* 2001, **105**, 4065; b) B. Nikoobakht, M. A. El-Sayed, *Chem. Mater.* 2003, **15**, 1957; c)W. Niu, S. Zheng, D. Wang, X. Liu, H. Li, S. Han, J. Chen, Z. Tang, G. Xu, *J. Am. Chem. Soc.* 2009, **131**, 697;

3   N. Tian, Z. Y. Zhou, S. G. Sun, Y. Ding, Z. L. Wang, *Science* 2007, **316**, 732.

4   J. Li, L. Wang, L. Liu, L. Guo, X. Han, Z. Zhang, *Chem. Commun.* 2010, **46**, 5109.

5   J. Zhang, M. R. Langille, M. L. Personick, K. Zhang, S. Li, C. A. Mirkin, *J. Am. Chem. Soc.* 2010, **132**, 14012

6   L. Zhang and C. Zhang, Nanoscale, 2013, 5, 5794.

7   F. Wang, C. Li, L. D. Sun, H. Wu, T. Ming, J. Wang, J. C. Yu, C. H. Yan, J. Am. Chem. Soc. 2011, 133, 1106.

8   a) E. Lantman, T. Deckert-Gaudig, Nat. Nanotechnol. 2012, 7, 583; b) W. Xie, C. Herrmann, K. Kompe, M. Haase, S. Schlucker, J. Am. Chem. Soc. 2011, 133, 19302. c) V. Joseph, C. Engelbrekt, J. Zhang, U. Gernert, Angew. Chem. Int. Ed. 2012, 51, 7592.